01 Apr 2013

Compact Object Coalescence Rate Estimation from Short Gamma-Ray Burst Observations

Carlo Enrico Petrillo

Alexander Dietz

Marco Cavaglia
Missouri University of Science and Technology, cavagliam@mst.edu

Recommended Citation

C. E. Petrillo et al., "Compact Object Coalescence Rate Estimation from Short Gamma-Ray Burst Observations," *Astrophysical Journal*, vol. 767, no. 2, Institute of Physics - IOP Publishing, Apr 2013.
The definitive version is available at https://doi.org/10.1088/0004-637X/767/2/140

The Astrophysical Journal, 767:140 (6pp), 2013 April 20 doi:10.1088/0004-637X/767/2/140

COMPACT OBJECT COALESCENCE RATE ESTIMATION FROM SHORT GAMMA-RAY BURST OBSERVATIONS

Carlo Enrico Petrillo[1], Alexander Dietz[2], and Marco Cavaglià[2]
[1] Dipartimento di Scienze Fisiche, Università di Napoli "Federico II," Compl. Univ. Monte S. Angelo, Ed. N, Via Cinthia, I-80126 Napoli, Italy
[2] Department of Physics and Astronomy, The University of Mississippi University, MS 38677-1848, USA
Received 2012 February 3; accepted 2013 March 10; published 2013 April 5

ABSTRACT

Recent observational and theoretical results suggest that short-duration gamma-ray bursts (SGRBs) originate from the merger of compact binary systems of two neutron stars or a neutron star and a black hole. The observation of SGRBs with known redshifts allows astronomers to infer the merger rate of these systems in the local universe. We use data from the *SWIFT* satellite to estimate this rate to be in the range ∼500–1500 Gpc^{-3} yr^{-1}. This result is consistent with earlier published results which were obtained through alternative approaches. We estimate the number of coincident observations of gravitational-wave signals with SGRBs in the advanced gravitational-wave detector era. By assuming that all SGRBs are created by neutron star–neutron star (neutron star–black hole) mergers, we estimate the expected rate of coincident observations to be in the range ≃0.2–1 (≃1–3) yr^{-1}.

Key words: gamma-ray burst: general – gravitational waves

Online-only material: color figures

1. INTRODUCTION

Short-duration gamma-ray bursts (SGRBs) are some of the most powerful explosions detected in the universe, releasing intensive bursts of high-energy gamma rays with a peak duration shorter than 2 s (Kouveliotou et al. 1993). The most commonly accepted explanation of their origin is a system of two compact objects, either two neutron stars (NS–NS) or a neutron star and a black hole (NS–BH) coalescing into a BH (Eichler et al. 1989; Narayan et al. 1992; Piro 2005; Rezzolla et al. 2011). Because of the emission of gravitational waves (GWs) during the latest phases of binary evolution, these objects are one of the primary sources for the next generation of ground-based GW detectors such as Advanced LIGO (Smith 2009) and Advanced Virgo (Acernese et al. 2008). Direct detection of a GW signal from a compact binary coalescing system would allow astronomers to gain valuable information on the astrophysics of compact objects, for example, the NS equation of state (Flanagan & Hinderer 2008; Read et al. 2009), as well as probe fundamental physics by testing the Lorentz invariance principle (Ellis et al. 2006) and general relativity in the strong-field regime (Will 2005), or by setting limits on the graviton mass (Stavridis & Will 2009; Keppel & Ajith 2010). Direct detection of a GW signal coinciding with a gamma-ray burst (GRB) optical counterpart could provide additional insights on astrophysics and even cosmology. The measure of the redshift of a GRB coinciding with a GW detection could allow astronomers to directly determine the distance of the system (see, e.g., Nissanke et al. 2010 and references therein). Coincident detections could also significantly improve the determination of the Hubble parameter by GW observations (Dalal et al. 2006; Del Pozzo 2011).

In this context, it is crucial to have reliable estimates of the local merger rate of compact objects and the number of expected coincident GW-SGRB observations in the advanced GW detector era. In this paper, we present a simple estimate of these quantities by using SGRB data from *SWIFT* observations.[3] In order to avoid selection bias, we calculate the number of expected coincident observations by restricting the sample of *SWIFT* data to observations with determined redshift and certain association to an optical counterpart. In contrast to a previous study by one of the authors (Dietz 2011), we also include the observed GRB luminosities in the analysis.

The paper is organized as follows. In Section 2, we define the *SWIFT* data sample and discuss the theoretical model that is used to fit the observations. In Section 3, we present the results and compare them to other published rate estimates. The Appendix contains details on the rate functions used in the analysis.

2. *SWIFT* DATA SAMPLE AND FITTING MODEL

We restrict our analysis to a set of SGRBs with reliable redshift measurement, i.e., to SGRBs that can be associated with a galaxy of known spectroscopic redshift with a high probability of being the host galaxy of the SGRB. We omit from the analysis SGRBs without an observed optical afterglow and SGRBs that are not associated with a host galaxy within the error circle of the observation. This allows us to remove any instrumental bias with respect to SGRBs detected by other missions. Table 1 shows a list of the 14 *SWIFT* SGRBs that pass our selection criteria.

The luminosity of these SGRBs can be computed using their redshift and fluence information. The fluence S is divided by the SGRB duration to estimate the flux F in the relevant frame for the detection threshold of the satellite (the observer frame). Since the observed fluence depends on the spectral properties of the source and the energy response of the detector (15–150 keV for the Burst Alert Telescope (BAT) instrument on board *SWIFT*; see Barthelmy et al. 2005), and the observations are over cosmological distances, two identical sources at different distances may show a spectral shift and a change of fluence. Expressing the observed photon number spectrum with the Band function (Band et al. 1993), this spectral shift can be calculated as a function of the redshift (Cao et al. 2011). Since most SGRB sources have redshift smaller than $z = 1$, the effect of the spectral shift is less than 10%

[3] http://heasarc.gsfc.nasa.gov/docs/swift/swiftsc.html

Table 1
List of the 14 SGRBs Observed by *SWIFT* between 2004 and 2011 which Pass Our Selection Criteria

GRB	Duration (s)	z	Type	Reference	Fluence (10^{-7} erg cm^{-2})
050416	2.0	0.6535	Emission	Cenko et al. (2005), Soderberg et al. (2007)	3.7 ± 0.4
051221	1.4	0.5465	Emission	Berger & Soderberg (2005), Soderberg et al. (2006)	11.5 ± 0.4
060502B	0.09	0.287	Absorption	Bloom et al. (2006), Bloom et al. (2007)	0.4 ± 0.1
060801	0.5	1.131	Emission	Cucchiara (2006), Berger et al. (2007)	0.8 ± 0.1
061006	130	0.4377	Emission	Berger et al. (2007)	14.2 ± 1.4
061201	0.8	0.111	Emission	Berger (2006), Stratta et al. (2007)	3.3 ± 0.3
070429B	0.5	0.9023	Emission	Perley et al. (2007), Cenko et al. (2008)	0.6 ± 0.1
070714B	64	0.9225	Emission	Graham et al. (2007), Cenko et al. (2008)	5.1 ± 0.3
071227	1.8	0.384	Emission	Berger et al. (2007), D'Avanzo et al. (2009)	2.2 ± 0.3
080905	1.0	0.1218	Emission	Rowlinson et al. (2010)	1.4 ± 0.2
090510	0.3	0.903	Emission	Rau et al. (2009), McBreen et al. (2010)	3.4 ± 0.4
100117	0.3	0.92	Emission	Fong et al. (2011)	0.9 ± 0.1
100816	2.9	0.8049	Absorption	Gorosabel et al. (2010)	20.0 ± 1.0
101219	0.6	0.718	Emission	Chornock & Berger (2011)	4.6 ± 0.3

Notes. The table shows the observed fluences, the redshifts, and the methods used to estimate the spectroscopic redshifts of the host galaxies. The fluence data are taken from Sakamoto et al. (2008; first seven SGBRs) and the Gamma-Ray burst Coordinated Network (http://gcn.gsfc.nasa.gov/gcn3_archive.html; last seven SGBRs: Barbier et al. 2007; Sato et al. 2007; Cummings et al. 2008; Ukwatta et al. 2009; Markwardt et al. 2010a, 2010b; Krimm et al. 2010, respectively). The unusual durations of the SGRB 061006 and 070714B are due to light curves with a short initial event followed by a softer extended event. They are classified as SGRBs (see Schady et al. 2006; Barbier et al. 2007). All SGRBs are preceded by an afterglow except 060502B, 060801, and 101219; however, only one galaxy was present in the error circle for these SGRBs.

(Cao et al. 2011). This error is small compared to other statistical and systematical errors and will be neglected in our analysis. The apparent luminosity of the SGRB is

$$L = 4\pi d_{\rm L}^2(z)\, F \simeq 4\pi d_{\rm L}^2(z) \frac{S}{T_{90}}\,, \tag{1}$$

where $d_{\rm L}(z)$ is the luminosity distance for a given redshift z, F is the mean flux, S is the measured fluence, and T_{90} is the time over which the burst emits 90% of its total energy. Throughout this paper, we consider a standard flat-Λ cosmology with $H_0 = 71$ km s^{-1}, $\Omega_M = 0.27$, and $\Omega_\Lambda = 0.73$. The left panel of Figure 1 shows the distribution of the observed luminosities as a function of the redshift. The solid line indicates the approximate detector's sensitivity threshold:

$$d_{\rm max}(L) = \sqrt{\frac{L}{4\pi F_{\rm lim}}}\,, \tag{2}$$

where the flux threshold is $F_{\rm lim} = 5 \times 10^{-9}$ erg s^{-1} cm^{-2} (Cao et al. 2011). The gray area in Figure 1 defines the so-called *redshift desert*, a region between $z \simeq 1$ and $z \simeq 2$ where spectroscopic redshift determinations are difficult to obtain (Fiore et al. 2007). In the following, we choose a conservative approach and further restrict our data sample to $z < 1$, leaving 13 data points for our analysis.

To determine the local merger rate, we fitted the sample with several commonly used luminosity functions (Dietz 2011; Chapman et al. 2009; Guetta & Stella 2008). The lognormal function and the Schechter function were found to provide acceptable fits. The cumulative distribution of the SGRBs as a function of the luminosity and the lognormal and Schechter functions are shown in Figure 1. Since the lognormal fit is slightly better than the Schechter fit, we restrict our analysis to the lognormal luminosity function

$$\phi(L) \propto \frac{1}{L} \exp\left(-\frac{\log L - \log L_0}{2\sigma^2}\right)\,, \tag{3}$$

where L_0 is the mean (peak) value of the luminosity and σ is the width of the distribution. These two parameters are determined by fitting the function to the 13 SGRBs in the sample. For the sake of simplicity, we do not consider evolutionary effects on the luminosity function. Although it is reasonable to assume that these effects are small compared to other statistical and systematical errors, some physical processes depend on the metallicity of the progenitors, which is a function of the redshift (Belczynski et al. 2010, 2011). The right panel of Figure 1 shows the cumulative distribution of SGRBs as a function of luminosity and the lognormal fit in Equation (3).

Since the fit is made on *observed* SGRBs, the luminosity function $\phi'(L)$ must be rescaled to the volume where *SWIFT* is sensitive. Assuming an isotropic distribution of SGRBs, we write

$$\phi(L) \propto \phi'(L)/d^3_{\rm max}(L)\,, \tag{4}$$

where $d^3_{\rm max}(L)$ is the maximum luminosity distance where an SGRB can be detected by *SWIFT*. The number of observable SGRBs within a redshift distance z is

$$N'(z) = N_0 \int_0^z dz' \frac{R(z')}{1+z'} \frac{dV(z')}{dz'} \int_{L_{\rm min}(z')}^{\infty} \phi(L) dL\,, \tag{5}$$

where $dV(z')/dz'$ is the comoving volume element and N_0 is a normalization factor. The rate function $R(z)$ describes the formation rate of the binary systems per comoving volume as a function of the redshift. Since a binary system of compact

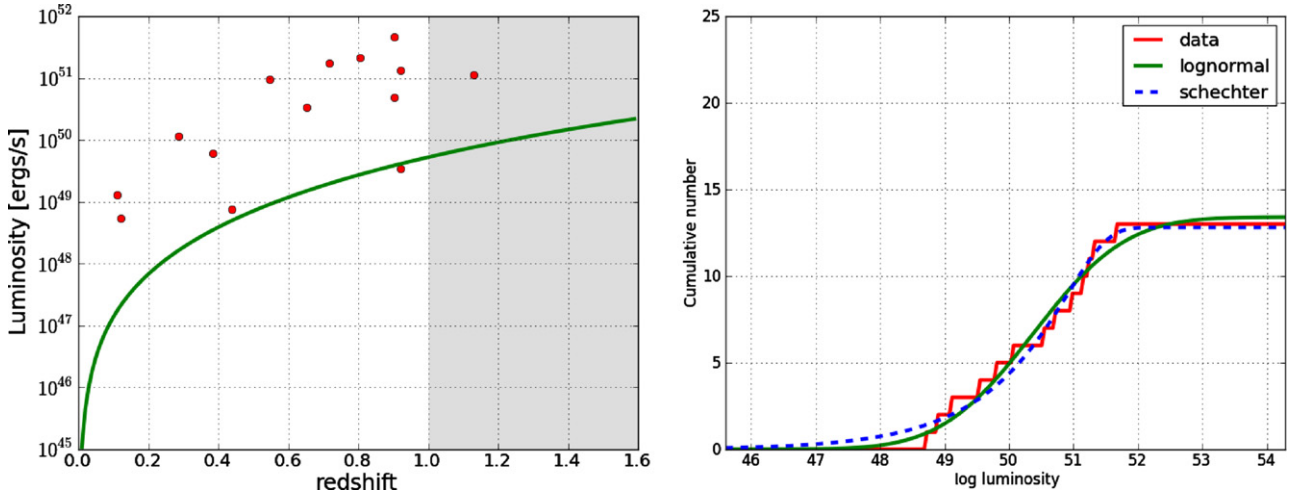

Figure 1. Left panel: luminosity distribution of the 14 SGRBs which pass the analysis selection criteria as function of their redshift. The gray area represents the *redshift desert*. Our analysis is restricted to the 13 SGRBs with $z < 1$. Right panel: cumulative distribution of the SGRBs as a function of luminosity (red), the lognormal function fit (green), and the Schechter function fit (dashed blue).

(A color version of this figure is available in the online journal.)

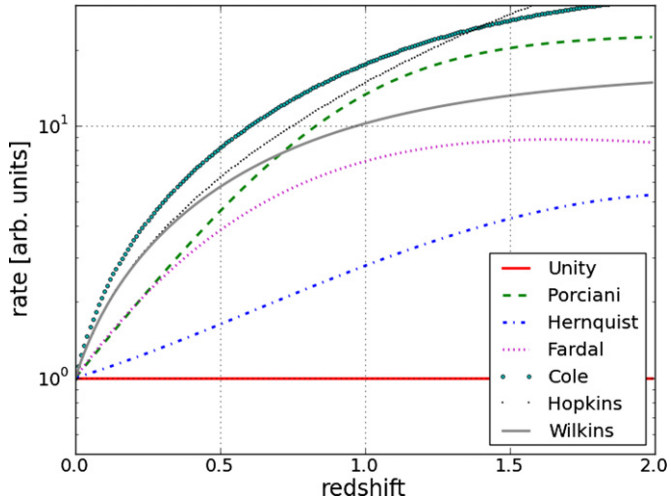

Figure 2. Different rate functions used in the analysis (see the Appendix for details). Note that the rate functions vary significantly even for redshift distances $z < 1$.

(A color version of this figure is available in the online journal.)

objects is formed from massive progenitor stars, $R(z)$ may be assumed to follow the star formation rate. The time difference from the formation of the compact objects to the coalescence of the binary is likely on the order of the Gyr (Belczynski et al. 2006). Thus, there is a significant delay with respect to the star formation rate. This is taken into account by using a delayed rate function in Equation (5). Figure 2 shows the different rate functions that are used in our analysis. The Appendix contains explicit expressions and references.

Since Equation (5) describes the number of SGRBs that may be potentially observed, $N'(z)$ must be rescaled to fit the number of SGRBs used in the analysis. From 2005 through 2011 ($T \simeq 6$ yr), *SWIFT* observed 46 SGRBs. (We neglect any downtime of the satellite due to technical issues or other constraints.) Thus, $N'(z)$ must be divided by the factor $f_R = 14/46$, with an estimated error of $\sqrt{14}/46 \sim 10\%$. The *SWIFT* field of view is about 1.4 sr (Barthelmy et al. 2005), corresponding to a visible fraction of the sky approximately equal to $f_{\rm FOV} \simeq 10\%$. Observations have shown that about 15% of all SGRBs may be created by soft gamma repeaters (SGRs; Nakar et al. 2006; Chapman et al. 2009). Since SGRs are typically less bright than ordinary SGRBs, events at larger redshifts might be composed mainly of SGRBs. If we assume that 85% of all SGRBs are created by the merger of two compact objects, the factor $f_{\rm SGR} = 0.85$ yields a conservative limit on the merger rate. In order to create a relativistic outflow, a torus must be created around the newly formed BH. Simulations and theoretical analyses show that the formation of a GRB depends on several parameters, such as the spin of the BH, the mass ratio of the binary, or the compactness of the NS (Pannarale et al. 2011; Rezzolla et al. 2011). Since these parameters are hard to generalize, we simply assume that all compact object mergers produce a GRB. GRBs are believed to emit their radiation in a collimated cone. The half-opening angle θ defines the fraction of the sky where the burst can be seen, $f_b = 1-\cos\theta$. The angle θ is highly uncertain, especially in the case of SGRBs, as it depends on the model and the Lorentz factor of the outflow (Panaitescu & Kumar 2001). Measurements of SGRB half-opening angles range from a few degrees to over 25° (Soderberg et al. 2004; Burrows et al. 2006; Grupe et al. 2006; Panaitescu 2006; Racusin et al. 2009). In the following, we set $1/f_b = 15$, corresponding to a half-opening angle $\theta \simeq 20°$ (Bartos et al. 2011). By taking into account all of these factors, the merger rate $R_{\rm merger}(z)$ and the expected rate of SGRB observations $R_{\rm SGRB}(z)$ are

$$R_{\rm merger}(z) = \frac{f_{\rm SGR}}{T\ f_b\ f_{\rm FOV}\ f_R} N'(z) \qquad (6)$$

and

$$R_{\rm SGRB}(z) = \frac{1}{T} N'(z)\,, \qquad (7)$$

respectively.

3. RESULTS AND DISCUSSION

The results of our analysis are summarized in Table 2. The approximate local merger rate of binary compact objects ranges from 479 to 1025 Gpc^{-3} yr^{-1}, depending on the chosen rate function. The upper limit comes from the model with unity rate function, which assumes no evolution on star formation over cosmological distances. The Porciani delayed rate function with

Table 2
Estimates of Merger Rates and Number of Detections Per Year for Advanced LIGO/Virgo

Rate Function	Merger Rate (Gpc^{-3} yr^{-1})	NS–NS Detections (yr^{-1})	NS–BH Detections (yr^{-1})
Unity	1025	525	3456
Hernquist	816	393	2750
Fardal	580	238	1954
Cole	485	170	1634
Hopkins	506	188	1706
Wilkins	553	206	1866
Porciani	479	196	1614
Porciani20	729	326	2457
Porciani100	757	340	2552

Notes. The detector reach is 450 Mpc for NS–NS binary systems and 930 Mpc for NS–BH binary systems. Results for different rate functions are shown. The Porciani20 and Porciani100 rate functions include delay times of 20 Myr and 100 Myr, respectively.

delay times of 20 Myr and 100 Myr gives merger rates about 50% larger than without the delay. Extrapolating this result to the other functions, a reasonable estimate for the merger rate in the local universe is in the range $\simeq$ 500–1500 Gpc^{-3} yr^{-1}. These results strongly depend on the half-opening angle of the SGRB jets. Figure 3 shows the dependence of the merger rate on the opening angle θ. The smaller the angle, the larger the number of mergers because the observer must be in the outflow cone to detect the SGRB. Assuming a half-opening angle of 10°, the merger rate could be as high as several thousand Mpc^{-3} yr^{-1}. A more isotropic large half-opening angle of 60° yields a rate of the order of 100 Mpc^{-3} yr^{-1}.

Assuming that a satellite with a field of view comparable to the field of view of *SWIFT* is operating at the time of advanced GW detectors, and using the expected range for Advanced LIGO/Virgo (LIGO Scientific Collaboration and Virgo Collaboration 2010), we can estimate the number of coincident observations of SGRBs with GW counterparts. Under the above assumptions, we estimate about 0.2–1 coincident observations per year for an NS–NS merger progenitor (detector range $\simeq$450 Mpc) and about 1–3 coincident observations per year for an NS–BH progenitor (detector range $\simeq$930 Mpc), a result consistent with earlier estimates (see Metzger & Berger 2012; Bartos et al. 2012 and references therein). These values include the systematic uncertainties underlying the estimates, as explained above. Since the advanced detectors are expected to operate for several years, a few observations of coincident SGRB-GW events seem likely.

These estimates could improve significantly with a network of operating GRB satellites. Assuming that *Fermi*[4] will be operating during the advanced detector era, as well as the planned SVOM mission (Paul et al. 2011) and Lobster,[5] the coincident SGRB-GW detection rate could be higher than the above estimate by a factor $\simeq$3. Ensuring that at least one GRB mission is operational at the time of advanced detectors will be crucial for identifying the host galaxy, measuring its redshift and star formation rate, and gaining valuable astrophysical information.

Our estimates can be compared to earlier published results that were obtained with alternative approaches. The two most common methods that are used to estimate the merger rate of compact objects rely on deriving the rates from observed pulsar observations (Kalogera et al. 2004) or employing population synthesis models (Belczynski et al. 2007). Both approaches inherit large statistical or systematical errors. A recent review article summarizes these results, concluding that the rate of merger events is somewhere between 10 and 10000 Gpc^{-3} yr^{-1} (LIGO Scientific Collaboration and Virgo Collaboration 2010). Other investigations rely on methods that are more similar to the method used here. Guetta & Piran (2005) use a sample of five SGRBs to estimate a merger rate in the range 8–30 Gpc^{-3} yr^{-1}. An earlier analysis by one of the authors, which is based on a less restrictive data sample and neglects individual GRB luminosities, yields a much higher rate of about 7800 Gpc^{-3} yr^{-1} (Dietz 2011). Finally, a recent study by Coward et al. (2012) uses a different method based on single GRB observations. In this approach, the maximum distance at which individual SGRBs can be detected by *SWIFT* is calculated and the results are then combined to estimate a final local rate of 0.16–1100 Gpc^{-3} yr^{-1}. These results show that our estimates are consistent with, and confirm, previous merger rate estimates. Future SGRB observations and improved statistics may further strengthen this conclusion.

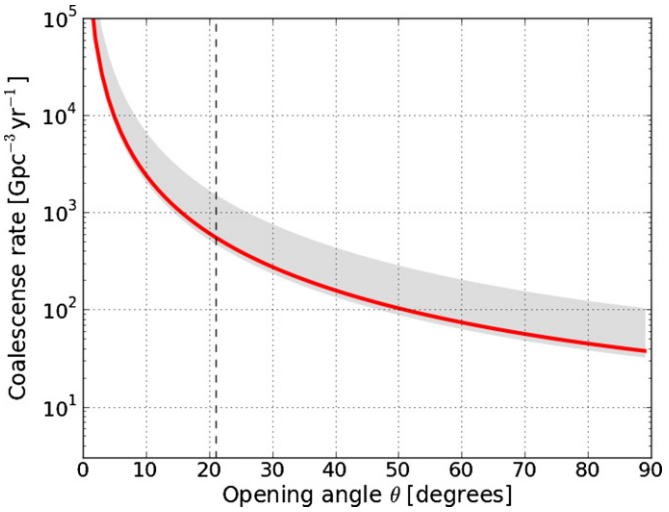

Figure 3. Merger rate of compact objects as a function of the half-opening angle θ. The red line indicates the median result. The gray area spans the possible range of rates due to different fit models and systematic errors. The vertical dashed line indicates the typical opening angle which is used in our estimate.
(A color version of this figure is available in the online journal.)

This work is the result of a Research Experience for Undergraduates (REU) project by Carlo Enrico Petrillo at the University of Mississippi. C.E.P., A.D., and M.C. are partially supported by the National Science Foundation through awards PHY-0757937 and PHY-1067985. The authors thank Jocelyn Read, Emanuele Berti, Maurizio Paolillo, Neil Gehrels, and Richard O'Shaughnessy for their help and valuable comments. This publication has been assigned LIGO Document Number LIGO-P1200015.

APPENDIX

RATE FUNCTIONS

This Appendix describes the various rate functions that are used in the analysis.

[4] http://fermi.gsfc.nasa.gov/
[5] N. Gehrels 2011, private communication.

Table 3
Parameters of the Cole Rate Function for Different Models in the Literature

Reference	a	b	c	d
Cole (Cole et al. 2001)	0.0166	0.1848	1.9474	2.6316
Hopkins (Hopkins & Beacom 2006)	0.0170	0.13	3.3	5.3
Wilkins (Wilkins et al. 2008)	0.014	0.11	1.4	2.2

Porciani. The Porciani rate function is the SF2 function in Porciani & Madau (2001):

$$R(z) \propto \frac{\exp(3.4\,z)}{\exp(3.4\,z)+22}\,. \tag{A1}$$

Hernquist. The Hernquist rate function is (Hernquist & Springel 2003)

$$R(z) \propto \frac{\chi^2}{1+\alpha(\chi-1)^3\exp(\beta\chi^{7/4})}\,, \tag{A2}$$

where

$$H(z) = H_0\sqrt{(1+z)^3\Omega_M+\Omega_\Lambda}\,,\ \chi(z) = \left[\frac{H(z)}{H_0}\right]^{2/3}\,, \tag{A3}$$

and $\alpha = 0.012$, $\beta = 0.041$.

Fardal. The Fardal rate function is defined as (Fardal et al. 2007)

$$R(z) \propto \frac{a^{-p_2}}{(1+p_1\,a^{-p_2})^{p_3+1}}H(z), \tag{A4}$$

where $p_1 = 0.075$, $p_2 = 3.7$, $p_3 = 0.84$, and $a = (1+z)^{-1}$.

Cole. The Cole rate function is

$$R(z) \propto \frac{a+bz}{1+(z/c)^d}H(z), \tag{A5}$$

where the parameters are summarized for different authors in Table 3.

Delayed functions. Since the time between the formation of the compact objects and the merger of the binary system is typically of the order of the Gyr, the merger rate may not follow directly from the star formation rate. Assuming a delay with respect to the star formation rate, the delayed rate function is defined as

$$R_t(z) = \int_0^{t_d} dt\,\frac{1}{1+z_f}R(z_{\rm ret})\,P(t)\,, \tag{A6}$$

where $P(t)$ represents the probability distribution of the delay time. Population synthesis models (Belczynski et al. 2001; Postnov & Yungelson 2005) suggest that this distribution is a power law

$$P(t) \propto t^{\alpha}\,, \tag{A7}$$

where $\alpha \simeq -1$ for $t > t_{\rm tmin}$. Although the observational literature has applied a much broader range of functional forms, a time delay probability distribution $P(t) \sim 1/t$ is sufficient for the purposes of this analysis, where binaries are produced in the field.[6] The retarded redshift, i.e., the redshift at the time when the compact objects are formed, is

$$z_{\rm ret} = T^{-1}(T(z)+t)\,. \tag{A8}$$

[6] R. O'Shaughnessy 2012, private communication.

The look-back time at redshift z is (see, e.g., Hogg 1999)

$$T(z) = T_0\int_0^{dz'}\frac{dz'}{(1+z')\sqrt{(\Omega_k(1+z')^3+\Omega_k(1+z')^2+\Omega_\Lambda)}}\,. \tag{A9}$$

The expression in Equation (A8) requires an integration and function inversion that generally need to be evaluated numerically. However, if flat cosmological models with $\Omega_k = 0$ are considered, then it is possible to obtain an analytic expression for the look-back time. Substituting

$$v = \Omega_k(1+z)^3 \tag{A10}$$

into Equation (A8), the integral takes the form

$$T(z) = \frac{T_0}{3}\int_{v(0)}^{v(z)} dv'\frac{1}{v\sqrt{v+\Omega_\Lambda}}\,. \tag{A11}$$

Integrating, it follows

$$T(z) = \frac{T_0}{3\sqrt{\Omega_\Lambda}}\left(L(v_0)-L(v_1)\right)\,, \tag{A12}$$

where

$$L(v) = \ln\left(\frac{\sqrt{v+\Omega_\Lambda}+\sqrt{\Omega_\Lambda}}{\sqrt{v+\Omega_\Lambda}-\sqrt{\Omega_\Lambda}}\right)\,. \tag{A13}$$

This analytic expression can be used to calculate the look-back time for a given redshift. Solving Equation (A12) for $L(v_1)$, we find

$$L(v_1) = L(v_0) - 3\sqrt{\Omega_\Lambda}\frac{T}{T_H} \equiv \ln E(T)\,. \tag{A14}$$

The value of $L(v_0)$ does not depend on z or T. Equation (A14) is a function of Ω_M and Ω_Λ, as one can see from Equations (A13) and (A10). Solving Equation (A13) for z, one finally obtains

$$z(T) = \left(\frac{\Omega_\Lambda}{\Omega_M}\right)^{1/3}\left[\left(\frac{1+E(T)}{1-E(T)}\right)^2-1\right]^{1/3}-1\,. \tag{A15}$$

REFERENCES

Acernese, F., Alshourbagy, M., Amico, P., et al. 2008, CQGra, 25, 184001
Band, D., Matteson, J., Ford, L., et al. 1993, ApJ, 413, 281
Barbier, L., Barthelmy, S. D., Cummings, J., et al. 2007, GCN, 6623, 1
Barthelmy, S. D., Barbier, L. M., Cummings, J. R., et al. 2005, SSRv, 120, 143
Bartos, I., Brady, P., & Marka, S. 2012, arXiv:1212.2289
Bartos, I., Finley, C., & Marka, S. 2011, PRL, 107, 251101
Belczynski, K., Bulik, T., Dominik, M., & Prestwich, A. 2011, arXiv:1106.0397
Belczynski, K., Dominik, M., Bulik, T., et al. 2010, ApJL, 715, L138
Belczynski, K., Kalogera, V., & Bulik, T. 2001, ApJ, 572, 407
Belczynski, K., Kalogera, V., Rasio, F. A., Taam, R. E., & Bulik, T. 2007, ApJ, 662, 504
Belczynski, K., Perna, R., Bulik, T., et al. 2006, ApJ, 648, 1110
Berger, E. 2006, GCN, 5952, 1
Berger, E., Fox, D. B., Price, P., et al. 2007, ApJ, 664, 1000
Berger, E., Morrell, N., & Roth, M. 2007, GCN, 7154, 1
Berger, E., & Soderberg, A. M. 2005, GCN, 4384, 1
Bloom, J. S., Perley, D., Kocevski, D., et al. 2006, GCN, 5238, 1
Bloom, J. S., Perley, D. A., Chen, H.-W., et al. 2007, ApJ, 654, 878
Burrows, D. N., Grupe, D., Capalbi, M., et al. 2006, ApJ, 653, 468
Cao, X.-F., Yu, Y.-W., Cheng, K., & Zheng, X.-P. 2011, MNRAS, 416, 2174
Cenko, S. B., Berger, E., Nakar, E., et al. 2008, arXiv:0802.0874
Cenko, S. B., Kulkarni, S. R., Gal-Yam, A., & Berger, E. 2005, GCN, 3542, 1
Chapman, R., Priddey, R. S., & Tanvir, N. R. 2009, MNRAS, 395, 1515
Chornock, R., & Berger, E. 2011, GCN, 11518, 1
Cole, S., Norberg, P., Baugh, C. M., et al. 2001, MNRAS, 326, 255

Coward, D., Howell, E., Piran, T., et al. 2012, MNRAS, 425, 1365
Cucchiara, A., Fox, D. B., Berger, E., & Price, P. A. 2006, GCN, 5470, 1
Cummings, J., Barthelmy, S. D., Baumgartner, W., et al. 2008, GCN, 8187, 1
Dalal, N., Holz, D. E., Hughes, S. A., & Jain, B. 2006, PhRvD, 74, 063006
D'Avanzo, P., Malesani, D., Covino, S., et al. 2009, A&A, 498, 711
Del Pozzo, W. 2011, arXiv:1108.1317
Dietz, A. 2011, A&A, 529, A97
Eichler, D., Livio, M., Piran, T., & Schramm, D. N. 1989, Natur, 340, 126
Ellis, J., Mavromatos, N., Nanopoulos, D., Sakharov, A., & Sarkisyan, E. 2006, A&A, 25, 402
Fardal, M. A., Katz, N., Weinberg, D. H., & Dav'e, R. 2007, MNRAS, 379, 985
Fiore, F., Guetta, D., Piranomonte, S., D'Elia, V., & Antonelli, L. A. 2007, A&A, 470, 515
Flanagan, É. É., & Hinderer, T. 2008, PhRvD, 77, 021502
Fong, W.-f., Berger, E., Chornock, R., et al. 2011, ApJ, 730, 26
Gorosabel, J., Castro-Tirado, A. J., Tanvir, N., et al. 2010, GCN, 11125, 1
Graham, J. F., Fruchter, A. S., Levan, A. J., et al. 2007, GCN, 6836, 1
Grupe, D., Burrows, D. N., Patel, S. K., et al. 2006, ApJ, 653, 462
Guetta, D., & Piran, T. 2005, A&A, 435, 421
Guetta, D., & Stella, L. 2008, A&A, 498, 329
Hernquist, L., & Springel, V. 2003, MNRAS, 341, 1253
Hogg, D. W. 1999, arXiv:astro-ph/9905116
Hopkins, A. M., & Beacom, J. F. 2006, ApJ, 651, 142
Kalogera, V., Kim, C., Lorimer, D. R., et al. 2004, ApJL, 601, L179
Keppel, D., & Ajith, P. 2010, PhRvD, 82, 122001
Kouveliotou, C., Meegan, C. A., Fishman, G. J., et al. 1993, ApJL, 413, L101
Krimm, H. A., Barthelmy, S. D., Baumgartner, W. H., et al. 2010, GCN, 11467, 1
LIGO Scientific Collaboration and Virgo Collaboration 2010, CQGra, 27, 173001
Markwardt, C. B., Barthelmy, S. D., Baumgartner, W. H., et al. 2010a, GCN, 10338, 1
Markwardt, C. B., Barthelmy, S. D., Baumgartner, W. H., et al. 2010b, GCN, 11111, 1
McBreen, S., Krühler, T., Rau, A., et al. 2010, A&A, 516, A71
Metzger, B., & Berger, E. 2012, ApJ, 746, 48
Nakar, E., Gal-Yam, A., & Fox, D. B. 2006, ApJ, 650, 281
Narayan, R., Paczynski, B., & Piran, T. 1992, ApJL, 395, L83
Nissanke, S., Holz, D. E., Hughes, S. A., Dalal, N., & Sievers, J. L. 2010, ApJ, 725, 496
Panaitescu, A. 2006, MNRAS, 367, L42
Panaitescu, A., & Kumar, P. 2001, ApJ, 571, 779
Pannarale, F., Tonita, A., & Rezzolla, L. 2011, ApJ, 727, 95
Paul, J., Wei, J., Basa, S., & Zhang, S.-N. 2011, CRPhy, 12, 298
Perley, D. A., Bloom, J. S., Modjaz, M., Poznanski, D., & Thoene, C. C. 2007, GCN, 7140, 1
Piro, L. 2005, Natur, 437, 822
Porciani, C., & Madau, P. 2001, ApJ, 548, 522
Postnov, K., & Yungelson, L. 2005, LRR, 9, 6
Racusin, J. L., Liang, E. W., Burrows, D. N., et al. 2009, ApJ, 698, 43
Rau, A., McBreen, S., & Kruehler, T. 2009, GCN, 9353, 1
Read, J. S., Markakis, C., Shibata, M., et al. 2009, PhRvD, 79, 124033
Rezzolla, L., Giacomazzo, B., Baiotti, L., et al. 2011, ApJL, 732, L6
Rowlinson, A., Wiersema, K., Levan, A. J., et al. 2010, MNRAS, 408, 383
Sakamoto, T., Barthelmy, S. D., Barbier, L., et al. 2008, ApJS, 175, 179
Sato, G., Barbier, L., Barthelmy, S. D., et al. 2007, GCN, 7148, 1
Schady, P., Burrows, D. N., Cummings, J. R., et al. 2006, GCN, 5699, 1
Smith, J. R. 2009, CQGra, 26, 114013
Soderberg, A. M., Berger, E., Kasliwal, M., et al. 2006, ApJ, 650, 261
Soderberg, A. M., Kulkarni, S. R., Berger, E., et al. 2004, Natur, 430, 648
Soderberg, A. M., Nakar, E., Cenko, S. B., et al. 2007, ApJ, 661, 982
Stavridis, A., & Will, C. M. 2009, PhRvD, 80, 044002
Stratta, G., D'Avanzo, P., Piranomonte, S., et al. 2007, A&A, 474, 827
Ukwatta, T. N., Barthelmy, S. D., Baumgartner, W. H., et al. 2009, GCN, 9337, 1
Wilkins, S. M., Trentham, N., & Hopkins, A. M. 2008, MNRAS, 385, 687
Will, C. M. 2005, LRR, 9, 3